

Shape Analysis of White Matter Tracts via the Laplace-Beltrami Spectrum

Lindsey Kitchell¹, Daniel Bullock¹, Soichi Hayashi¹, and Franco Pestilli¹

¹ Indiana University, Bloomington IN 47405, USA
kitchell@indiana.edu | franpest@indiana.edu

Abstract. Diffusion-weighted magnetic resonance imaging (dMRI) allows for non-invasive, detailed examination of the white matter structures of the brain. White matter tract specific measures based on either the diffusion tensor model (e.g. FA, ADC, and MD) or tractography (e.g. volume, streamline count or density) are often compared between groups of subjects to localize differences within the white matter. Less commonly examined is the shape of the individual white matter tracts. In this paper, we propose to use the Laplace-Beltrami (LB) spectrum as a descriptor of the shape of white matter tracts. We provide an open, automated pipeline for the computation of the LB spectrum on segmented white matter tracts and demonstrate its efficacy through machine learning classification experiments. We show that the LB spectrum allows for distinguishing subjects diagnosed with bipolar disorder from age and sex matched healthy controls, with classification accuracy reaching 95%. We further demonstrate that the results cannot be explained by traditional measures, such as tract volume, streamline count, or mean and total length. The results indicate that there is valuable information in the anatomical shape of the human white matter tracts.

Keywords: Shape Analysis, White Matter, Laplace Beltrami spectrum.

1 Introduction

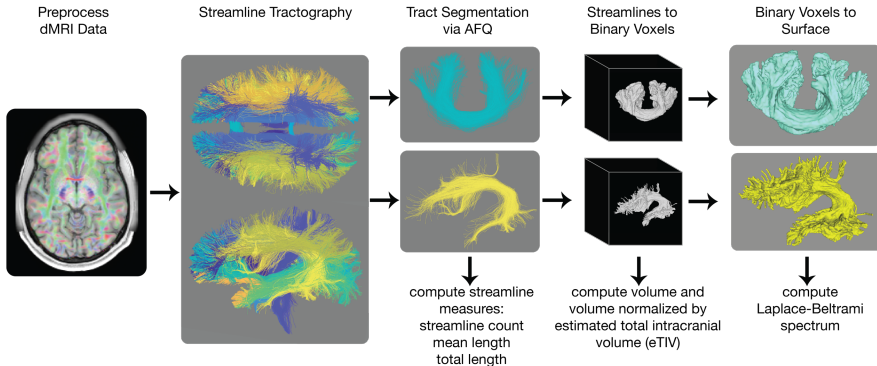
The development of diffusion-weighted magnetic resonance imaging (dMRI) has allowed for non-invasive, detailed examination of the white matter structures of the brain. Diffusion tensor imaging (DTI) models the diffusion of water molecules within the tissue of the white matter and provides measures that describe the tissue's microstructure and organization. These measures (such as fractional anisotropy, apparent diffusion coefficient, and mean diffusivity, among others) are often compared between groups of subjects, such as individuals with a neurological disorder and matched healthy controls, to localize differences within the white matter. Tractography can be applied in combination with the dMRI data to map the putative path of neuronal fiber bundles (streamlines) within the white matter. These maps are generally referred to as tractograms and they can be segmented into major white matter tracts. Tract-specific measures (such as volume, streamline density, or streamline count) are also often compared between groups, as well as the diffusion measures along the streamlines. Less commonly examined however, is the anatomical shape of the individual white matter tracts.

Although there are several popular methods for the shape analysis of brain structures (e.g. medial representations, spherical harmonics, deformation-based morphometry, and spectral methods [1,2,3,4]), very few have been applied to the segmented tracts of the white matter. This may be because streamlines, rather than a solid structure, are used to represent the white matter tracts, making it difficult to conceptualize the tracts as anatomical objects and to apply the more common brain shape methods. Several techniques specific to the streamline representation of white matter tracts have been developed [e.g. 5, 6, 7], however, they may have issues with proper correspondence. These methods typically try to establish correspondence either between the points along the streamlines within a tract or between the streamlines of tracts of different individuals. This can be problematic, as pointed out in Durrleman et al. [8], because it has never been shown that the points on a streamline or the streamlines themselves are homologous anatomical structures. Rather, it is the entire white matter tract that is the homologous structure across populations. Thus, it may be suggested that methods for analyzing the shape of white matter tracts should not rely on point or streamline correspondence, but should instead focus on the boundary and overall shape of the tract.

In this paper, we propose to use the Laplace-Beltrami spectrum as a global shape descriptor of white matter tracts. The Laplace-Beltrami spectrum is isometry invariant and does not require the establishment of correspondence [4,9]. As such, it can be used to describe the boundary and general shape of the individual tracts (once converted from streamlines to a surface representation) without any registration or alignment. Additionally, the computation of the Laplace-Beltrami spectrum can be automated, making it ideal for large scale analyses, and applied to segmented tracts generated using any tractography algorithm, including probabilistic, deterministic, or ensemble methods. The Laplace-Beltrami spectrum has previously been used for the shape analysis of brain structures [e.g. 4,10,11,12,13], however we believe this is the first study to apply it to segmented white matter tracts. We developed an automated pipeline (Figure 1) for computing the Laplace-Beltrami spectrum on white matter tracts and make it available as open source code and as cloud-based open services at brainlife.io (see Table 1). We demonstrate the efficacy of the Laplace-Beltrami spectrum as a shape descriptor for white matter tracts using machine learning classification. We show that the Laplace-Beltrami spectrum allows for distinguishing with high accuracy between healthy controls (age and sex matched) and subjects diagnosed with bipolar disorder from the UCLA Consortium for Neuropsychiatric Phenomics LA5c Study [14]. Research on bipolar disorder has consistently demonstrated an association with abnormalities in the white matter [15]. We compare the shape-based results to analyses using volume and other tract-specific measures (e.g. total streamline count, mean length of streamlines, and total length of streamlines). Our results demonstrate that the shape of the human white matter tracts contains important information that allows for the characterization of human individuality and variability between groups of subjects. We show that the Laplace-Beltrami spectrum, when applied to white matter tracts, can be used for discriminating, with high accuracy, between healthy controls and individuals diagnosed with neuropsychiatric disorders.

Table 1. Links to GitHub repositories and Brainlife.io applications for each step of the pipeline.

Processing Step	GitHub repository	Brainlife.io application
Preprocessing of dMRI data	github.com/brain-life/app-datanormalize github.com/brain-life/app-splitshells github.com/brain-life/app-dtiinit	https://brainlife.io/app/59272453436ee50ffd669a08 https://brainlife.io/app/592db717b3cd7c00211dc230 https://brainlife.io/app/58c56cf7e13a50849b258800
Freesurfer	github.com/brain-life/app-freesurfer	https://brainlife.io/app/58c56d92e13a50849b258801
Ensemble tracking	github.com/brain-life/app-ensembletracking	https://brainlife.io/app/592dbbccb3cd7c00211dc235
Tract segmentation	github.com/brain-life/app-AFQ_no-life	https://brainlife.io/app/59dff93521ff360021b24ebf
Segmentation cleaning	github.com/brain-life/app-AFQclean	https://brainlife.io/app/597f8c463a37c7002e39bf77
Binary voxel generation	github.com/kitchell/app-generatetratractmasks	https://brainlife.io/app/592dc03eb3cd7c00211dc239
Surface generation	github.com/kitchell/app-generatetractsurfaces	https://brainlife.io/app/593049d7ff090a00210eff05
LB spectrum	github.com/kitchell/app-LBspectrum_matlab	https://brainlife.io/app/5a53b2be56e507002d1a9628
Streamline measures	github.com/kitchell/app-classifiedfibertractstats	https://brainlife.io/app/599f2c0a1a12b6002f642c74
Tract volume	github.com/kitchell/app-binvolvolume	https://brainlife.io/app/5afe0f2a2e93b90028263655

**Fig. 1.** Automated pipeline for shape analysis of white matter tracts.

2 Methods

2.1 Data and Preprocessing

Diffusion-weighted (dMRI) and T1-weighted structural MRI (sMRI) data from the UCLA Consortium for Neuropsychiatric Phenomics LA5c Study [14] were used for this study. We used data from 43 individuals diagnosed with bipolar disorder and 43 age and sex matched controls. The dMRI (spatial resolution of 2 mm³ and 64 directions) images were aligned to corresponding sMRI, AC-PC aligned, anatomical images, and we utilized the 1,000 s/mm² b-value acquisition shell. Freesurfer was used to segment the T1-weighted image into different tissue types and brain regions [16] and all subsequent analyses were performed within the white matter tissue.

2.2 Automated Pipeline for White Matter Tract Shape Analysis

Tractography generation. For this paper, ensemble tractography methods [17,18,19] were used to generate a whole brain tractogram of 615,000 streamlines by seeding

within the entire white matter segmentation [20]. We combined both probabilistic and deterministic tracking methods, across a range of L_{\max} (2-8), a range of curvature (0.25, 0.5, 1, 2, 4), and a fixed step size of 0.2 mm.

Tract segmentation. Twenty major white matter tracts (9 bi-hemispheric and 2 cross-hemispheric tracts) were segmented using established atlases and segmentation techniques from the Automated Fiber Quantification software (AFQ) [21]. The two cross-hemispheric tracts were the callosum forceps major and callosum forceps minor. The nine bi-hemispheric tracts (18 individual tracts) consisted of the right and left arcuate, cingulum cingulate, cingulum hippocampus, corticospinal, inferior fronto-occipital fasciculus (IFOF), inferior lateral fasciculus (ILF), super lateral fasciculus (SLF), thalamic radiation, and uncinate. An automated cleaning method provided by AFQ was applied to the segmentations to remove stray streamlines that deviate substantially from the core white matter tract path.

Binary voxel and surface generation. To generate surface representations of the segmented white matter tracts, the streamline representations of each tract were first converted into a binary voxel representation. The data was resampled to a higher resolution (2 mm^3 to 0.7 mm^3) in order to create a smoother, more detailed tract. For each streamline comprising the tract, we recorded which voxels of the resampled image contained a streamline node. A smoothing kernel was applied to ensure that the volume was a spatially contiguous, non-porous object. Because this smoothing has the unintended consequence of inflating the object, we removed a proportion of the lowest density voxels (20%). Additionally, a simple masking step was performed with a node count threshold and we removed all voxels with less than 2 nodes. The resulting volume was then passed to the surface generation component of the process.

A discrete marching cubes algorithm was applied to each binary voxel representation to create a triangular surface mesh. The surface was then smoothed for 10 iterations using a windowed sinc function interpolation kernel (a standard signal processing low-pass filter) [22]. This filter essentially relaxed the mesh, making the triangular faces better shaped and the vertices more evenly distributed. After smoothing, any non-connected components of the surface (islands) were removed.

Shape descriptor computation. The Laplace-Beltrami (LB) spectrum was used as a shape descriptor of the surface mesh of each white matter tract. The LB spectrum allows for highly discriminative shape comparisons with minimal preprocessing [4,9]. Importantly, the eigenvalues estimated from the LB spectrum are isometry invariant, therefore requiring no registration or mapping between the surfaces of different tracts or subjects. The eigenvalues of the Laplace-Beltrami operator, Δ , were computed using the first-order finite element method by solving the Laplacian eigenvalue problem on each given surface:

$$\Delta f = -\lambda f. \quad (1)$$

The solution consists of a number (n) of eigenvalue ($\lambda_i \in \mathbb{R}$) and eigenfunction (f_i) pairs, sorted by the eigenvalue magnitude ($0 \leq \lambda_1 \leq \lambda_2 \leq \dots$). To achieve scale independence and allow a direct shape comparison between tracts irrespective of size, we normalized the eigenvalues by the surface area of the given tract, also known as the Riemannian volume v [9]:

$$\lambda' = vol^{-1/2}\lambda. \quad (2)$$

The normalized LB spectrum was computed on the triangle mesh surfaces of all 20 segmented white matter tracts for all subjects. Similar to spherical harmonics [2], the more eigenvalues included in the spectrum, the more details of the shape are represented (Figure 2). Because the complexity of the shape of each tract varies widely, we used a range of non-zero eigenvalues of the LB spectrum, dependent on the tract, for the analyses in this paper. All computations of the LB spectrum were done in MatLab (Mathworks, Natick, MA) using the Geometry Processing Toolbox [23].

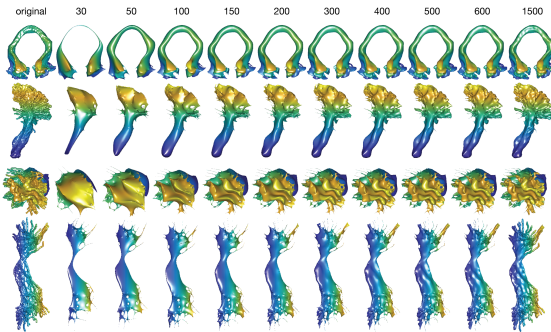


Fig. 2. White matter tracts reconstructed with different amounts of eigenfunctions. The original tract surface is shown in the leftmost column, followed by the tract reconstructed with the number of eigenvalues listed above (30–1500). Top. Callosum forceps minor tract, superior view. Middle. Left corticospinal tract, anterior and superior view. Bottom. Left IFOF tract, left view. Color = z-coordinate of the vertices (yellow – superior, blue – inferior).

Volume and streamline measures computation. The volume of each white matter tract was computed using the resampled binary voxel representation. To compute the total volume of a tract, the volume of a single voxel was determined based on the resolution of the resampled dMRI data (7mm^3) and then multiplied by the total number of voxels in the binary voxel representation. The volume was also divided by the estimated total intracranial volume (eTIV) as calculated by FreeSurfer [16], to normalize for brain size. Analyses were performed on both the normalized and non-normalized volumes. Additionally, the total number of streamlines, average length of streamlines, and total combined length of the streamlines were computed based on the segmented streamline representation of each tract.

2.3 Statistical Analysis

Permutation tests (20,000 permutations for all tests) were used to compare the volume, streamline measures and eigenvalue spectrums of each segmented white matter tract between the disorder groups and their age/sex matched controls. For the volume and streamline measure values a two-sided, nonparametric, permutation test based on the t-statistic was used. Individual eigenvalues were also compared using independent, two-sided, nonparametric permutation tests, as done in [4,13], and the false discovery rate method of correction was used to correct for multiple comparisons.

2.4 Machine Learning Experiments

Binary classification (bipolar disorder vs. healthy control) was performed using machine learning algorithms implemented in the Python package scikit-learn [24]. We performed five different machine learning experiments: (1) classification using only the (non-normalized) volume values as features, (2) classification using only the streamline measures as features, (3) classification using the combined LB spectrums of all tracts as features, (4) classification using the LB spectrum of single tracts as features individually, and (5) voting-based ensemble classification based on the results of (4). To prepare the data for classification, we standardized each feature by removing the mean and scaling the values to unit variance. This standardization procedure ensured that each feature had the properties of a standard normal distribution, a requirement for many of the algorithms.

Because this is an initial, exploratory study, we performed an exhaustive grid search using 10-fold cross validation across 7 different machine learning classifier algorithms and classifier hyperparameter sets for each experiment (RandomForestClassifier (RF), AdaBoostClassifier (ABC), SVC (SVM, C-Support Vector Classification), KNeighborsClassifier (KNN), DecisionTreeClassifier (DT), LinearDiscriminantAnalysis (LDA), LogisticRegression (LR) in scikit-learn [24]). In the experiments using the LB spectrum, we also performed the grid search across numbers of eigenvalues (30, 50, 100, 150, 200, 300, 400, 500, 600). The results of the grid search helped us determine which classification algorithms and hyperparameter sets performed best for each feature set, as well as which level of shape detail (number of eigenvalues of the LB spectrum) allowed for the greatest distinction between the two groups. For experiments (1) through (4), the best performing classifier and hyperparameter set was used for a final classification with leave-one-out (LOO) cross validation, repeated 10 times. LOO cross validation was used for the final classification due to the relatively limited number of subjects available in the data set. The average accuracy, sensitivity (true positive rate) and specificity (true negative rate) of the classifications are reported.

For experiment (5), we developed a robust voting-based ensemble classification method that combined the results of the series of weaker classifiers applied to individual white matter tracts in experiment (4) [25]. The results of experiment (4) identified the best performing eigenvalue, classifier, and hyperparameter set for each tract. The classification also provided a predicted classification category (vote) for each subject in the

dataset (bipolar disorder or control). The final classification for this experiment is obtained by setting the final category of each subject to the mode of the vote distribution (predicted classification category distribution) across the tracts. In the case of a tie, a null category was reported. This voting-based classification was performed 10 times.

3 Results

3.1 Statistical analysis

We performed a series of control analyses to show whether the white matter tracts differed between the two groups in a series of properties, such as volume, streamline counts, and length. Results show that only two of the white matter tracts had a statistically significant difference in non-normalized volume between the controls (C) and subjects with bipolar disorder (BD): the right cingulum cingulate ($p=0.044$, BD>C) and the right uncinate ($p=0.021$, C>BD). Of the normalized volume (volume/eTIV) comparison, only the right uncinate was statistically significant ($p=0.007$, C>BD). Four tracts had a statistically significant difference in streamline count between the two groups: the left cingulum hippocampus ($p=0.015$, BD>C), the left corticospinal tract ($p=0.020$, C>BD), the right corticospinal tract ($p=0.013$, C>BD), and the right uncinate ($p=0.005$, C>BD). One tract had a statistically significant group difference in mean length: the left ILF ($p=0.005$, BD>C). Three tracts had a statistically significant difference in total length between the two groups: the right cingulum cingulate ($p=0.048$, BD>C), the left cingulum hippocampus ($p=0.016$, BD>C), and the right uncinate ($p=0.016$, C>BD).

We also tested whether single eigenvalues of the individual white matter tracts differed between the two groups. Results of the permutation tests for the eigenvalues are shown in Figure 3. The right and left cingulum hippocampus, the right and left corticospinal, and the right uncinate all had multiple eigenvalues with p-values that passed the 5% and 15% FDR correction for multiple comparisons, suggesting significant shape differences between the two groups for those tracts. The right arcuate, right SLF, and the right and left ILF had eigenvalues with p-values that passed the 15% FDR correction for multiple comparisons.

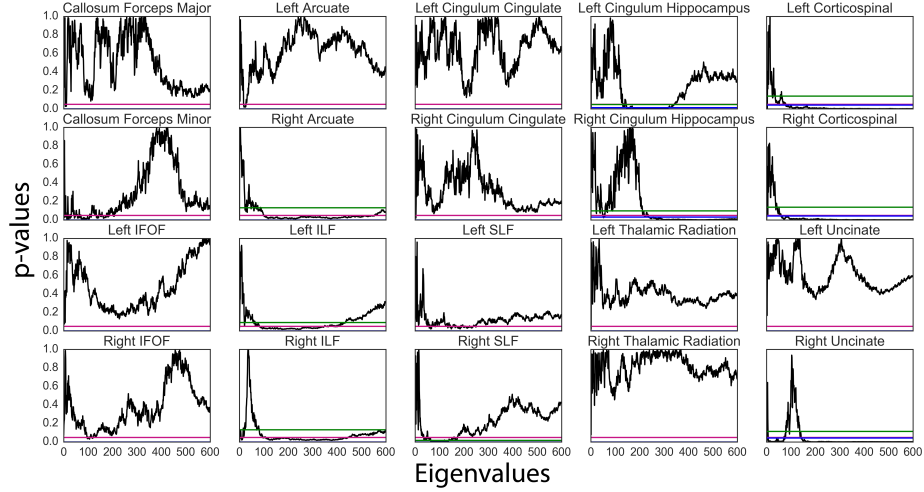


Fig. 3. Results of the permutation tests for the individual eigenvalues of the Laplace-Beltrami spectrum. The p-value of each eigenvalue is plotted for each tract. Red horizontal lines are the 0.05 significance level. If any of the eigenvalues passed FDR correction the FDR significance level is plotted in green (15% FDR) and blue (5% FDR).

3.2 Machine learning classification

(1) Binary classification using volume only. For this experiment, we used the non-normalized volume only. The input feature set was 20 volume values for each subject. Using the best classifier and hyperparameter set as determined by the grid search (KNeighborsClassifier), a final classification was performed. The classification accuracy was 54.65%, with a sensitivity of 37.20%, and specificity of 79.09%. The results were the same for all 10 repeats.

(2) Binary classification streamline measures only. For this experiment, the input feature set was 20 streamline counts, 20 mean length values, and 20 total length values for each subject. Using the best classifier and hyperparameter set as determined by the grid search (LogisticRegression), a final classification was performed. The classification accuracy was 70.56%, with a sensitivity of 69.76% and specificity of 72.09%. The results were the same for all 10 repeats. Overall classification and specificity was significantly improved using the streamline measures over the volume measures, although specificity was slightly reduced.

(3) Binary classification using the Laplace-Beltrami spectrum of all tracts. For these experiments, the input features were the n -number of eigenvalues times 20 tracts across nine different numbers of eigenvalues. The LogisticRegression classifier performed the best in the grid search for all eigenvalue numbers, and therefore was the classifier used for the final classification of all eigenvalue numbers. The results of the final classification using the best performing hyperparameter sets for each eigenvalue

number are shown in Table 2. The highest obtained average accuracy was 67.79% (± 1.34) with 200 eigenvalues, a sensitivity of 67.90% (± 0.63), and specificity of 67.67% (± 0.87). Overall classification accuracy using the combined LB spectrums of all tracts was better than classification using only the volumes of tracts, but slightly worse than classification using just the streamline measures.

Table 2. Classification results using the combined LB spectrums of all tracts (Experiment 3).

# eigenvalues	30	50	100	150	200	300	400	500	600
Accuracy	62.67 (± 2.01)	58.13 (± 1.09)	62.79 (± 0.00)	64.76 (± 1.23)	67.79 (± 1.34)	65.58 (± 0.98)	65.11 (± 0.00)	62.09 (± 0.81)	61.97 (± 0.95)
Sensitivity	67.67 (± 1.19)	65.11 (± 0.66)	65.11 (± 0.00)	67.90 (± 0.42)	67.90 (± 0.63)	61.16 (± 0.48)	60.46 (± 0.00)	59.53 (± 0.51)	58.60 (± 0.63)
Specificity	57.67 (± 0.91)	51.11 (± 0.47)	60.46 (± 0.00)	61.62 (± 0.70)	67.67 (± 0.87)	70.00 (± 0.73)	69.76 (± 0.00)	64.65 (± 0.78)	65.34 (± 0.56)

(4) Binary classification using the Laplace-Beltrami spectrum of single tracts. For these experiments, we performed the final binary classification of each individual tract using the eigenvalue, classifier, and hyperparameter sets that performed best in the grid search. The eigenvalue, average classification accuracy, sensitivity, and specificity of each tract are shown in Figures 4 and 5. The best overall classification accuracy obtained with a single tract, the left corticospinal tract, was 77.79% (± 1.15) (sensitivity = 85.34% (± 1.56), specificity = 70.23% (± 1.47)), followed by the left arcuate at 76.74% (± 0.00) (sensitivity = 79.06% (± 0.00), specificity = 74.41% (± 0.00)) and the callosum forceps minor at 74.88% (± 0.12) (sensitivity = 73.95 % (± 0.21), specificity = 75.81% (± 0.12)). All but one of the white matter tracts achieved an overall accuracy higher than volume based classification ($>54\%$), 6 of the individual tracts achieved an overall accuracy higher than streamline measures based classification ($>70\%$) and 10 achieved an overall accuracy higher than classification based on the combined LB spectrums of all tracts ($>67\%$).

(5) Voting-based ensemble classification using the Laplace-Beltrami spectrum of each tract. For this experiment, we used the results of experiment (4) for a voting-based classification. Each tract was used to predict the classification category of each subject. The mode of the classification predictions (votes) across all tracts was computed to assign a final classification category to each subject. The average overall classification accuracy was 95.23% (± 0.03), significantly higher than the accuracy of the 4 previous experiments. The average sensitivity was 95.34% (± 0.00) and average specificity was 95.11% (± 0.06). The average classification accuracy, sensitivity, and specificity are also shown in Figures 4 and 5.

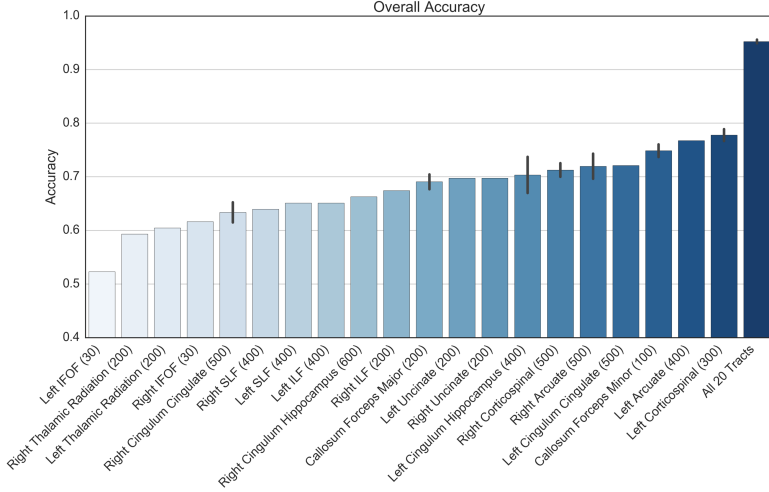


Fig. 4. Average overall accuracy of the classification based on the LB spectrum of individual white matter tracts (Experiment 4) and of the voting-based ensemble classification (Experiment 5), sorted in order of overall accuracy. Black lines represent the standard deviation across the 10 classification repeats; bars with no line had the same result for all repeats. Eigenvalue used for the final classification is listed in parentheses.

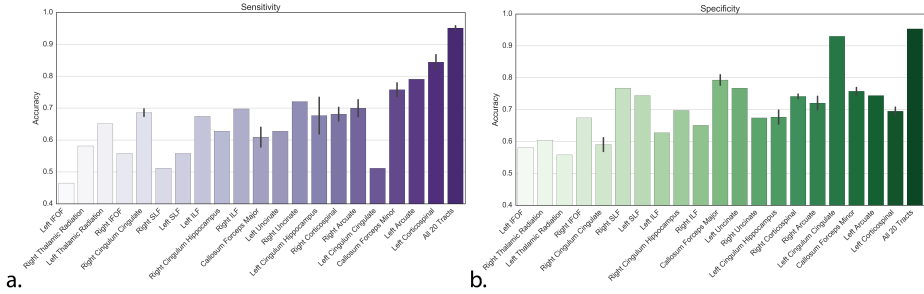


Fig. 5. (a) Average overall sensitivity (true positive rate) and (b) specificity (true negative rate) of the classification based on the LB spectrum of individual white matter tracts (Experiment 4) and of the voting-based ensemble classification (Experiment 5), sorted in the same order as Figure 4. Black lines represent the standard deviation across the 10 classification repeats; bars with no line had the same result for all repeats.

4 Discussion and Conclusion

In this paper, we proposed the Laplace-Beltrami spectrum be used as a global shape descriptor of white matter tracts. Using the LB spectrum, volume, and streamline measures of segmented white matter tracts, we compared the efficacy of each feature for distinguishing subjects diagnosed with bipolar disorder from age and sex matched controls. Results showed that the shape of the white matter tracts contains important

information that allows for a more accurate classification between the two groups. Machine learning classification performed using the LB spectrums of single tracts achieved higher classification accuracy than the volume or streamline measure-based classifications, with 6 of the tracts reaching an overall accuracy above 70%. The individual tract with the highest classification accuracy was the left corticospinal, followed by the left arcuate (comparable to the results of [26]), and the callosum forceps minor. Overall classification accuracy was significantly improved when using a voting-based classification method with the LB spectrums, reaching 95% overall accuracy, 95% sensitivity, and 95% specificity.

Our results illustrate the importance of including shape information in neuroanatomical and neuropsychiatric research for a more complete picture of disorder related differences in the brain. Of the top three performing tracts in the shape classification (all >74% in overall accuracy), only one, the left corticospinal tract, had a significant difference in any of the non-shape measures (streamline count). None of the three had any statistical difference in volume, mean or total streamline length. Analyses based only on volume or streamline measures might mistakenly conclude that there are no disorder related differences in those tracts.

The high classification accuracy we obtained demonstrates that the LB spectrum captures meaningful information about white matter tract morphology. The results suggest that including the shape of white matter tracts in neuropsychiatric research may be useful for narrowing down the etiology of the range of neuropsychiatric and brain disorders known to be accompanied by changes in the white matter [15]. Future research directions include expanding the analyses to incorporate other neuropsychiatric disorders, such as schizophrenia and attention deficit hyperactivity disorder, as well as including comparisons to analyses with diffusion-based microstructure measures.

Acknowledgements

This research was supported by NSF IIS-1636893, NSF BCS-1734853, NIH NIMH ULTR001108, and a Microsoft Research Award, the Indiana University Areas of Emergent Research initiative “Learning: Brains, Machines, Children”, the Pervasive Technology Institute and the Research Technologies Division of University Information Technology Services at Indiana University. The authors thank Yu Wang and Justin Solomon who provided insight and expertise on the Laplace-Beltrami operator.

References

1. Styner, M., et al. (2003). Statistical shape analysis of neuroanatomical structures based on medial models. *Medical image analysis* 7(3): 207-220.
2. Styner, M., et al. (2006). Framework for the statistical shape analysis of brain structures using SPHARM-PDM. *The insight journal* (1071): 242.
3. Ashburner, J. and K. J. Friston (2000). Voxel-based morphometry—the methods. *Neuroimage* 11(6): 805-821.
4. Niethammer, M., et al. (2007). Global medical shape analysis using the Laplace-Beltrami spectrum. *International Conference on Medical Image Computing and Computer-Assisted Intervention*, Springer.

5. Corouge, I., et al. (2004). A statistical shape model of individual fiber tracts extracted from diffusion tensor MRI. *International Conference on Medical Image Computing and Computer-Assisted Intervention*, Springer.
6. O'Donnell, L. J., et al. (2009). Tract-based morphometry for white matter group analysis. *Neuroimage* **45**(3): 832-844.
7. Glazman, T., et al. (2018). Framework for shape analysis of white matter fiber bundles. *Neuroimage* **167**: 466-477.
8. Durrleman, S., et al. (2011). Registration, atlas estimation and variability analysis of white matter fiber bundles modeled as currents. *Neuroimage* **55**(3): 1073-1090.
9. Reuter, M., et al. (2006). Laplace-Beltrami spectra as ‘Shape-DNA’ of surfaces and solids. *Computer-Aided Design* **38**(4): 342-366.
10. Shi, Y., et al. (2009). Inverse-consistent surface mapping with Laplace-Beltrami eigen-features. *International Conference on Information Processing in Medical Imaging*, Springer.
11. Wachinger, C., Golland, P., Kremen, W., Fischl, B., Reuter, M., & Alzheimer's Disease Neuroimaging Initiative. (2015). BrainPrint: a discriminative characterization of brain morphology. *NeuroImage*, **109**, 232-248.
12. Wachinger, C., et al. (2016). Whole-brain analysis reveals increased neuroanatomical asymmetries in dementia for hippocampus and amygdala. *Brain* **139**(12): 3253-3266.
13. Shishegar, R., et al. (2011). Hippocampal shape analysis in epilepsy using Laplace-Beltrami spectrum. *Electrical Engineering (ICEE)*, 2011 19th Iranian Conference on, IEEE.
14. Poldrack, R. A. et al. A genome-wide examination of neural and cognitive function. *Sci. Data* **3**:160110 doi: 10.1038/sdata.2016.110 (2016).
15. Fields, R. D. (2008). White matter in learning, cognition and psychiatric disorders. *Trends in neurosciences*, **31**(7), 361-370.
16. Fischl B. (2012). FreeSurfer. *NeuroImage*, **62**:774-781
17. Takemura, H., Caiafa, C. F., Wandell, B. A., & Pestilli, F. (2016). Ensemble tractography. *PLoS computational biology*, **12**(2), e1004692.
18. Caiafa, C. F., & Pestilli, F. (2017). Multidimensional encoding of brain connectomes. *Scientific reports*, **7**(1), 11491.
19. Pestilli, F., Yeatman, J. D., Rokem, A., Kay, K. N., & Wandell, B. A. (2014). Evaluation and statistical inference for human connectomes. *Nature methods*, **11**(10), 1058.
20. Tournier, J. D., Calamante, F., & Connelly, A. (2012). MRtrix: diffusion tractography in crossing fiber regions. *International Journal of Imaging Systems and Technology*, **22**(1)
21. Yeatman, J. D., Dougherty, R. F., Myall, N. J., Wandell, B. A., & Feldman, H. M. (2012). Tract profiles of white matter properties: automating fiber-tract quantification. *PloS one*, **7**(11), e49790.
22. Taubin, G., Zhang, T., & Golub, G. (1996). Optimal surface smoothing as filter design. In *European Conference on Computer Vision* (pp. 283-292). Springer, Berlin, Heidelberg.
23. Alec Jacobson and others (2016) gptoolbox: Geometry Processing Toolbox. <http://github.com/alecjacobson/gptoolbox>
24. Pedregosa F., Varoquaux, G., Gramfort, A., Michel, V., Thirion, B., Grisel, O., Blondel, M., Prettenhofer, P., Weiss, R., Dubourg, V., Vanderplas, J., Passos, A., Cournapeau, D., Brucher, M., Perrot, M., Duchesnay, E. Scikit-learn: Machine Learning in Python, *Journal of Machine Learning Research*, **12**, 2825-2830 (2011)
25. Dietterich, T. G. (2000, June). Ensemble methods in machine learning. In *International workshop on multiple classifier systems* (pp. 1-15). Springer, Berlin, Heidelberg.
26. Sun, Z. Y., Houenou, J., Duclap, D., Sarrazin, S., Linke, J., Daban, C., ... & Delavest, M. (2017). Shape analysis of the cingulum, uncinate and arcuate fasciculi in patients with bipolar disorder. *Journal of psychiatry & neuroscience: JPN*, **42**(1)